Light manipulation by dual channel storage in ultra-cold Rydberg medium

Xue-Dong Tian(田雪冬)[1], Zi-Jiao Jing(景梓骄)[1], Feng-Zhen Lv(吕凤珍)[1], Qian-Qian Bao(鲍倩倩)[2,†], and Yi-Mou Liu(刘一谋)[3,‡]

[1] *College of Physics Science and Technology, Guangxi Normal University, Guilin* 541004, *China*
[2] *College of Physics, Liaoning University, Shenyang* 110036, *China*
[3] *Center for Quantum Sciences and School of Physics, Northeast Normal University, Changchun* 130024, *China*

(Received 12 July 2022; revised manuscript received 19 September 2022; accepted manuscript online 23 September 2022)

We investigate the light propagation dynamics in ultra-cold Rydberg medium with inverted-Y configuration based on the superatom theory. It is viable to store light information in two types of atomic spin coherence (trivial spin coherence and Rydberg spin coherence), which makes the system a prospective platform for versatile light manipulation. A normal feature is to realize efficient light storage with simultaneous resonant control fields applied. An intriguing feature is to split light into two beams with different intensities and statistical properties if the control fields are applied separately. The beam of light retrieved from the Rydberg spin coherence is severely attenuated and shows anti-bunching character accompanied by the cooperative optical nonlinearity. Moreover, generation and manipulation of beating signal are achievable by applying the non-resonant control fields.

Keywords: Rydberg atom, electromagnetically induced transparency, light storage, dark-state polariton

PACS: 42.50.–p, 32.80.Ee, 42.50.Gy **DOI:** 10.1088/1674-1056/ac946c

1. Introduction

Photons are the prospective carriers for quantum information owing to the fast velocity, but it is still a herculean task to directly control photons or obtain effective interactions between photons.[1] Electromagnetically induced transparency (EIT) is a well-known quantum coherence effect that can suppress resonant absorption to achieve nonlinearity and to reduce the group velocity of propagation pulse to zero to attain the light storage.[2] With the EIT technique, one can map the quantum state of the slowly propagating photons into the stationary wave packet of spin coherence in the atomic medium, thus the desirable control of photons can be realized by manipulating the atomic coherence.[3,4] Many schemes based on EIT-medium have been proposed to achieve manipulation of light in atomic ensembles, e.g., light storage and retrieval,[5,6] generation of beating signals,[7,8] and stationary light pulses.[9,10]

Rydberg-EIT medium[11–13] is also a promising tool for light manipulation, which provides an efficient way for transferring photons to Rydberg excitations. The long-range dipole–dipole interaction between Rydberg atoms will be mapped to the photons in turn, enabling to obtain effective photon–photon interaction.[14] The large interaction between Rydberg atoms will cause the dipole-blockade effect, which makes Rydberg-EIT medium exhibit enhanced optical nonlinearity.[15,16] Owing to this, Rydberg medium has emerged as a platform to realize quantum gate,[17–20] entanglement,[21–25] bound state,[26,27] and quantum devices,[28–31] including single-photon sources, switches, transistors, and absorbers. Recently, light propagation and storage in Rydberg-EIT medium[32–38] have been realized experimentally. In these experiments, nonlinear manipulation of photons can be achieved via the conversion between Rydberg spin coherence and the photons. Some theoretical methods,[39–44] e.g, effective field theory (EFT) and superatom (SA) theory, to simulate the propagation and storage processes have also been proposed. In Ref. [42], an SA model is applied to study light storage and retrieval process in a Rydberg atomic medium with three-level ladder configuration. The retrieved field energy exhibits the saturation effect against the input field energy accompanied by the anti-bunching feature. Apart from the Rydberg atomic medium with ladder configuration, the media with other complex configurations, which show the combination behaviors of the regular EIT and the Rydberg EIT,[45,46] have attracted some attention owing to the flexibility of coherent optical control. However, the studies are restricted to the steady-state optical response such as normal[45] and abnormal nonlinear EIT.[46] Considering the dynamic response, it is viable to achieve multiple manipulations of light such as splitting the light into beams with different intensities and statistical properties and generating beating signal. To realize the multiple light manipulations, we present an approach based on the atomic system with inverted-Y configuration showing the combination behaviors of the regular

†Corresponding author. E-mail: baoqianqian@lnu.edu.cn
‡Corresponding author. E-mail: liuym605@nenu.edu.cn

© 2023 Chinese Physical Society and IOP Publishing Ltd

EIT and the Rydberg EIT. We focus on how to make the system exhibit different behaviors to realize different kinds of light manipulation.

We adopt the SA theory to simulate the light propagation dynamics in the Rydberg atomic ensemble. By modulating the control fields, a part of light propagates in the formation of trivial dark-state polariton (TDP) while the other part of light propagates as the Rydberg dark-state polariton (RDP). Switching off the control fields means to store light in the trivial and Rydberg atomic spin coherence. Owing to the different storage and retrieval channels, the system can exhibit trivial EIT behavior or Rydberg EIT behavior only by adjusting the control fields, then it is viable to realize the dynamic manipulation of light in the following ways during the retrieval process. Firstly, we will retrieve the stored light that is not severely attenuated if the resonant control fields are applied simultaneously during the retrieval process. Secondly, two beams of light with different intensities and statistical properties will be released at different times if the control fields are applied separately, which can be explored to implement the beam splitter. The light retrieved from the Rydberg spin coherence experiences serious loss and shows the cooperative optical nonlinearity arising from the dipole-blockade effect. Thirdly, generation of beating signal is achievable by applying the nonresonant control fields. Adjusting the detunings of the control fields can help to manipulate the beating frequency.

2. Model and equations

Here we consider a cloud of atomic gas envisioned as a one-dimensional medium (length L) with the four-level inverted-Y configuration (as shown in Fig. 1). The medium interacts with a weak quantum probe field $\hat{E}_{\rm p}(z,t) = \sqrt{\frac{\hbar\omega_{\rm p}}{2\varepsilon_0 V}}\hat{\mathcal{E}}_{\rm p}(z,t)\,{\rm e}^{{\rm i}(k_{\rm p}z-\omega_{\rm p}t)} + {\rm h.c.}$ with the central frequency $\omega_{\rm p}$ (the amplitude $\hat{\mathcal{E}}_{\rm p}(z,t)$) and two strong classical control fields with the central frequencies $\omega_{\rm c}$ and $\omega_{\rm d}$ ($E_{\rm c}(z,t) = \mathcal{E}_{\rm c}(t)\,{\rm e}^{{\rm i}(k_{\rm c}z-\omega_{\rm c}t)} + {\rm h.c.}$ and $E_{\rm d}(z,t) = \mathcal{E}_{\rm d}(t)\,{\rm e}^{{\rm i}(k_{\rm d}z-\omega_{\rm d}t)} + {\rm h.c.}$), respectively; k_ζ is the projection of the wave vector of the corresponding field along z direction with $\zeta \in \{{\rm p},{\rm c},{\rm d}\}$. The probe field with Rabi frequency $\hat{\Omega}_{\rm p}(z,t) = g\hat{\mathcal{E}}_{\rm p}(z,t)$ couples the atomic ground state $|g\rangle$ to a short-lived excited state $|e\rangle$, with $g = \wp_{ge}\sqrt{\omega_{\rm p}/(2\hbar\varepsilon_0 V)}$ being the single-photon coupling strength, $\wp_{ge}$ the electric dipole moment of transition $|g\rangle \leftrightarrow |e\rangle$, V the local quantum volume ($V = AL$), and A the cross section area of both the quantum field mode and the atomic medium. The control field with Rabi frequency $\Omega_{\rm c}(t) = \mathcal{E}_{\rm c}(t)\wp_{me}/2\hbar$ ($\Omega_{\rm d}(t) = \mathcal{E}_{\rm d}(t)\wp_{\rm er}/2\hbar$) couples the excited state $|e\rangle$ to a metastable state $|m\rangle$ (a long-lived highly excited Rydberg state $|r\rangle$), where $\wp_{me}$ ($\wp_{\rm er}$) is the electric dipole moment of transition $|m\rangle \leftrightarrow |e\rangle$ ($|e\rangle \leftrightarrow |r\rangle$). The detunings between the fields and the transitions are $\Delta_{\rm p} = \omega_{\rm p} - \omega_{eg}$, $\Delta_{\rm c} = \omega_{\rm c} - \omega_{em}$ and $\Delta_{\rm d} = \omega_{\rm d} - \omega_{re}$, respectively, where $\omega_{eg,em,re}$ represent the atomic transition frequencies. The decay rates of states $|e\rangle$ and $|r\rangle$ are $2\gamma_e$ and $2\gamma_r$, respectively. In the following discussion, we will adopt $\hat{P}(z,t) = \sqrt{N}\hat{\bar{\sigma}}_{ge}(z,t)$ to describe the slowly varying polarization, $\hat{S}_1(z,t) = \sqrt{N}\hat{\bar{\sigma}}_{gm}(z,t)$ and $\hat{S}_2(z,t) = \sqrt{N}\hat{\bar{\sigma}}_{gr}(z,t)$ to describe the spin fields, with N being the atomic volume density and $\hat{\bar{\sigma}}_{ge}(z,t) = \frac{1}{N_z}\sum_j^{N_z}\hat{\sigma}_{ge}^j\,{\rm e}^{-{\rm i}k_{\rm p}z_j}$ ($\hat{\bar{\sigma}}_{gm}(z,t) = \frac{1}{N_z}\sum_j^{N_z}\hat{\sigma}_{gm}^j\,{\rm e}^{-{\rm i}(k_{\rm p}-k_{\rm c})z_j}$, $\hat{\bar{\sigma}}_{gr}(z,t) = \frac{1}{N_z}\sum_j^{N_z}\hat{\sigma}_{gr}^j\,{\rm e}^{-{\rm i}(k_{\rm p}+k_{\rm d})z_j}$) being average atomic transition operator in the small volume ΔV centered at z_j. Here $\hat{\sigma}_{\mu\nu}^j = |\mu_j\rangle\langle\nu_j|$ represents single atomic transition operator for jth atom with N_z being the number of atoms at position z_j ($\mu,\nu \in \{g,e,m,r\}$ and $\mu \neq \nu$).

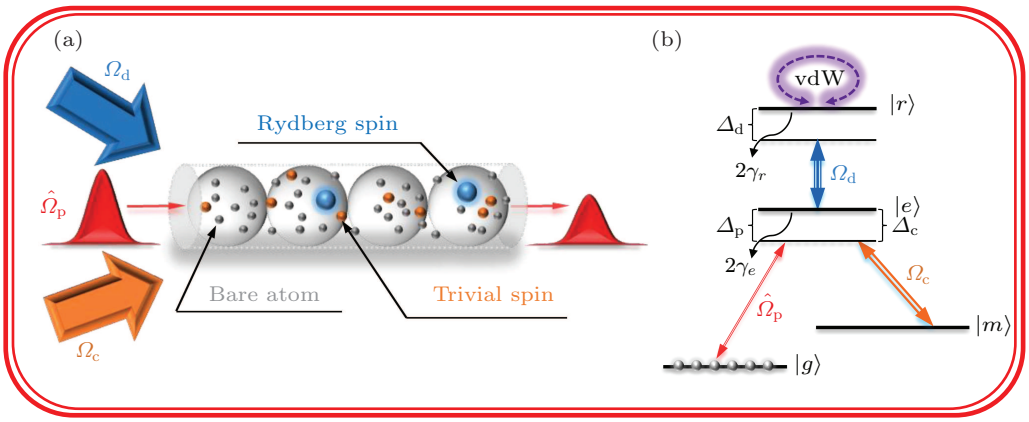


Fig. 1. (a) Schematic illustration of the probe pulse propagating in a sample of cold Rydberg atoms envisioned as a collection of SAs. (b) Schematic of a four-level inverted-Y system of interacting cold ^{87}Rb atoms driven by two classical control fields $\Omega_{\rm c}$ and $\Omega_{\rm d}$ and one quantum probe field $\hat{\Omega}_{\rm p}$.

In the limit of very low atomic excitations ($\langle\hat{\sigma}_{gg}\rangle \to 1$), the relative operators $(\hat{\mathcal{E}},\hat{P},\hat{S}_1,\hat{S}_2)$ satisfy the same-time bosonic commutation relations in Ref. [47]. If a pair of atoms located at z_i and z_j are excited to the Rydberg state $|r\rangle$ simultaneously, they will interact through the van der Walls (vdW) potential $\Delta(z_i - z_j) = C_6/|z_i - z_j|^6$. Then we can write down the corresponding Hamiltonians:

$$\hat{H} = \hat{H}_{\rm p} + \hat{H}_{\rm ap} + \hat{H}_{\rm int},$$

$$
\begin{aligned}
\hat{H}_{\rm p} &= \frac{{\rm i}\hbar c}{L}\int_0^L {\rm d}z\hat{\mathcal{E}}_{\rm p}^{\dagger}(z,t)\,\partial_z\hat{\mathcal{E}}_{\rm p}(z,t),\\
\hat{H}_{\rm ap} &= -\hbar\int_0^L {\rm d}z[\Delta_{\rm p}\hat{P}^{\dagger}(z,t)\hat{P}(z,t)\\
&\quad +\Delta_1\hat{S}_1^{\dagger}(z,t)\hat{S}_1(z,t)+\Delta_2\hat{S}_2^{\dagger}(z,t)\hat{S}_2(z,t)]\\
&\quad -\hbar\int_0^L {\rm d}z[g\sqrt{N}\hat{\mathcal{E}}_{\rm p}^{\dagger}(z',t)\hat{P}(z,t)\\
&\quad +\Omega_{\rm c}^{*}(t)\hat{S}_1^{\dagger}(z,t)\hat{P}(z,t)\\
&\quad +\Omega_{\rm d}(t)\hat{S}_2^{\dagger}(z,t)\hat{P}(z,t)+{\rm h.c.}],\\
\hat{H}_{\rm int} &= \frac{\hbar}{2}\int_0^L {\rm d}z\int_0^L {\rm d}z'\hat{S}_2^{\dagger}(z,t)\hat{S}_2^{\dagger}(z',t)\\
&\quad \times\Delta(z-z')\hat{S}_2(z',t)\hat{S}_2(z,t),
\end{aligned}
\tag{1}
$$

where $\hat{H}$ denotes the total Hamiltonian of the system while $\hat{H}_{\rm p}$, $\hat{H}_{\rm ap}$ and $\hat{H}_{\rm int}$ are the kinetic term, atom-field coupling term and the vdW interaction term, respectively, with $\Delta_1=\Delta_{\rm p}-\Delta_{\rm c}$ and $\Delta_2=\Delta_{\rm p}+\Delta_{\rm d}$.

Using Hamiltonian $\hat{H}$, we obtain Heisenberg–Langevin equations for the field $\hat{\Omega}_{\rm p}(z,t)$, the polarization and the spin field operators $\hat{P}(z,t)$, $\hat{S}_1(z,t)$, and $\hat{S}_2(z,t)$:

$$
\begin{aligned}
\partial_t\hat{P}(z,t) &= -[\gamma_e-{\rm i}\Delta_{\rm p}]\hat{P}(z,t)+{\rm i}\Omega_{\rm c}(t)\hat{S}_1(z,t)\\
&\quad +{\rm i}\Omega_{\rm d}^{*}(t)\hat{S}_2(z,t)+{\rm i}\sqrt{N}\hat{\Omega}_{\rm p}(z,t),\\
\partial_t\hat{S}_1(z,t) &= {\rm i}\Delta_1\hat{S}_1(z,t)+{\rm i}\Omega_{\rm c}^{*}(t)\hat{P}(z,t),\\
\partial_t\hat{S}_2(z,t) &= -\left[\gamma_r-{\rm i}\left(\Delta_2-\langle\hat{\Delta}_{\rm s}\rangle\right)\right]\hat{S}_2(z,t)+{\rm i}\Omega_{\rm d}(t)\hat{P}(z,t),\\
\partial_t\hat{\Omega}_{\rm p}(z,t) &= -c\partial_z\hat{\Omega}_{\rm p}(z,t)+{\rm i}g^2V\sqrt{N}\hat{P}(z,t),
\end{aligned}
\tag{2}
$$

where $\hat{\Delta}_{\rm s}=\frac{1}{2}\int {\rm d}z'\hat{S}_2^{\dagger}(z',t)\Delta(z-z')\hat{S}_2(z',t)$ refers to the vdW-induced frequency shift, making Eq. (2) difficult to solve. To deal with this dilemma, we consider all $n_{\rm sa}=NV_{\rm sa}$ atoms in the blockade sphere $V_{\rm sa}=4\pi R_{\rm b}^3/3$ as an SA, with radius $R_{\rm b}\approx[C_6\gamma_e/(|\Omega_{\rm c}(t)|^2+|\Omega_{\rm d}(t)|^2]^{1/6}$. In the mean-field approximation, for the atoms in the SA with an assured Rydberg excitation, the average vdW-induced frequency shift $\langle\hat{\Delta}_{\rm s}\rangle$ tends to infinity, indicating that these atoms behave like a three-level Λ system which decouples from state $|r\rangle$. On the contrary, for the atoms in an SA without a Rydberg excitation, $\langle\hat{\Delta}_{\rm s}\rangle$ tends to be negligible, which manifests that these atoms behave like the four-level inverted-Y system. Moreover, the interactions among different SAs are generally too weak to be considered. Thus the dynamic evolution of each atom should be the combination of three-level and four-level systems and the proportions for these two systems are merely subject to the probability for a single Rydberg excitation occurring in the SAs. Regarding this, we can obtain the dynamic equations for the polarization and spin fields:

$$
\begin{aligned}
\partial_t\hat{P}^{(4)}(z,t) &= -[\gamma_e-{\rm i}\Delta_{\rm p}]\hat{P}^{(4)}(z,t)\\
&\quad +{\rm i}\Omega_{\rm c}(t)\hat{S}_1^{(4)}(z,t)+{\rm i}\Omega_{\rm d}^{*}(t)\hat{S}_2^{(4)}(z,t)\\
&\quad +{\rm i}\sqrt{N}\hat{\Omega}_{\rm p}(z,t),\\
\partial_t\hat{S}_1^{(4)}(z,t) &= {\rm i}\Delta_1\hat{S}_1^{(4)}(z,t)+{\rm i}\Omega_{\rm c}^{*}(t)\hat{P}^{(4)}(z,t),\\
\partial_t\hat{S}_2^{(4)}(z,t) &= -\left[\gamma_r-{\rm i}\left(\Delta_2-\langle\hat{\Delta}_{\rm s}\rangle\right)\right]\hat{S}_2^{(4)}(z,t)\\
&\quad +{\rm i}\Omega_{\rm d}(t)\hat{P}^{(4)}(z,t),
\end{aligned}
\tag{3}
$$

for the four-level inverted-Y system, and

$$
\begin{aligned}
\partial_t\hat{P}^{(3)}(z,t) &= -[\gamma_e-{\rm i}\Delta_{\rm p}]\hat{P}^{(3)}(z,t)+{\rm i}\Omega_{\rm c}(t)\hat{S}_1^{(3)}(z,t)\\
&\quad +{\rm i}\sqrt{N}\hat{\Omega}_{\rm p}(z,t),\\
\partial_t\hat{S}_1^{(3)}(z,t) &= {\rm i}\Delta_1\hat{S}_1^{(3)}(z,t)+{\rm i}\Omega_{\rm c}^{*}(t)\hat{P}^{(3)}(z,t),
\end{aligned}
\tag{4}
$$

for the three-level Λ system.

Next, we will consider the dynamics of individual SA in terms of collective states and operators to calculate the single Rydberg excitation probability in each SA. The ground state is expressed as $|G\rangle=|g\rangle^{\otimes n_{\rm sa}}$, and single Rydberg collective excited state is $\left|R^{(1)}\right\rangle=(1/\sqrt{n_{\rm sa}})\sum_i^{n_{\rm sa}}|g_1,\ldots,r_i,\ldots,g_{n_{\rm sa}}\rangle$, with other collective states

$$
\begin{aligned}
|E^{(j)}\rangle &= \frac{\left[\sum_{\mu=1}^{n_{\rm sa}}\hat{\sigma}_{eg}^{\mu}{\rm e}^{{\rm i}k_{\rm p}z_\mu}\right]^j}{\sqrt{n_{\rm sa}!j!/(n_{\rm sa}-j)!}}|G\rangle,\quad |M^{(j)}\rangle=\frac{\left[\sum_{\mu=1}^{n_{\rm sa}}\hat{\sigma}_{mg}^{\mu}\cdot{\rm e}^{{\rm i}(k_{\rm p}-k_{\rm c})z_\mu}\right]^j}{\sqrt{n_{\rm sa}!j!/(n_{\rm sa}-j)!}}|G\rangle,\\
|E^{(j)}R^{(1)}\rangle &= \frac{\left[\sum_{\mu=1}^{n_{\rm sa}}\hat{\sigma}_{eg}^{\mu}\cdot{\rm e}^{{\rm i}k_{\rm p}z_\mu}\right]^j\cdot\sum_{\mu=1}^{n_{\rm sa}}\hat{\sigma}_{rg}^{\mu}\cdot{\rm e}^{{\rm i}(k_{\rm p}+k_{\rm d})z_\mu}}{\sqrt{n_{\rm sa}!j!/(n_{\rm sa}-j-1)!}}|G\rangle,\quad |M^{(j)}R^{(1)}\rangle=\frac{\left[\sum_{\mu=1}^{n_{\rm sa}}\hat{\sigma}_{mg}^{\mu}\cdot{\rm e}^{{\rm i}(k_{\rm p}-k_{\rm c})z_\mu}\right]^j\cdot\sum_{\mu=1}^{n_{\rm sa}}\hat{\sigma}_{rg}^{\mu}\cdot{\rm e}^{{\rm i}(k_{\rm p}+k_{\rm d})z_\mu}}{\sqrt{n_{\rm sa}!j!/(n_{\rm sa}-j-1)!}}|G\rangle,\\
|E^{(s)}M^{(j)}R^{(1)}\rangle &= \frac{\left[\sum_{\mu=1}^{n_{\rm sa}}\hat{\sigma}_{eg}^{\mu}\cdot{\rm e}^{{\rm i}k_{\rm p}z_\mu}\right]^s\left[\sum_{\mu=1}^{n_{\rm sa}}\hat{\sigma}_{mg}^{\mu}\cdot{\rm e}^{{\rm i}(k_{\rm p}-k_{\rm c})z_\mu}\right]^j\cdot\sum_{\mu=1}^{n_{\rm sa}}\hat{\sigma}_{rg}^{\mu}\cdot{\rm e}^{{\rm i}(k_{\rm p}+k_{\rm d})z_\mu}}{\sqrt{n_{\rm sa}!s!j!/(n_{\rm sa}-s-j-1)!}}|G\rangle,
\end{aligned}
\tag{5}
$$

containing at most one Rydberg excitation.

We define the operators $\hat{\Sigma}_{IJ}=|I\rangle\langle J|$ to describe the collective transition ($I\neq J$) or projection ($I=J$) for SAs, where $\hat{\Sigma}_{IJ}=\hat{\Sigma}_{JI}^{\dagger}$ with $\{I,J\}\in\{G,R^{(1)},M^{(j)},E^{(j)},E^{(j)}R^{(1)},M^{(j)}R^{(1)},E^{(s)}M^{(j)}R^{(1)},\ldots\}$ and $s,j\in\{1,2,\ldots\}$. The SA projection operator $\hat{\Sigma}_{RR}$ should be specially attended, which is indispensable for obtaining the effective probe polarizability conditioned upon the Rydberg excitation. In the weak probe limit, that is merely contributed by state $|\hat{R}^{(1)}\rangle$ with written as $\hat{\Sigma}_{RR}\simeq\hat{\Sigma}_{RR}^{(1)}=|\hat{R}^{(1)}\rangle\langle\hat{R}^{(1)}|$,

whose expected value can be calculated through Eqs. (A1) and (A2). However, in the general case, other higher-order collective states ($|\hat{E}^{(1)}\hat{R}^{(1)}\rangle$, $|\hat{M}^{(1)}\hat{R}^{(1)}\rangle$, $|\hat{E}^{(1)}\hat{M}^{(1)}\hat{R}^{(1)}\rangle$, ...) are also essential to evaluate Rydberg excitation $\hat{\Sigma}_{RR} \simeq \hat{\Sigma}^{(1)}_{RR} + \hat{\Sigma}^{(2)}_{RR} + \hat{\Sigma}^{(3)}_{RR} + \cdots$ [see Appendix A].

We can write down the conditional probe polarizability:

$$\hat{P}(z,t) = \hat{P}^{(3)}(z,t)\langle\hat{\Sigma}_{RR}(z,t)\rangle + \hat{P}^{(4)}(z,t)(1-\langle\hat{\Sigma}_{RR}(z,t)\rangle). \quad (6)$$

By solving the coupling Eqs. (3)–(6), it is possible to attain the dynamic evolution of the probe field:

$$\partial_z\Omega_{\rm p}(z,t) = {\rm i}g^2V\sqrt{N}P(z,t), \quad (7)$$

with $O(z,t) = \langle\hat{O}(z,t)\rangle$ representing the expectation value of operator $\hat{O}(z,t)$. In addition, we have removed the time derivative ∂_t, which is negligibly in the slow-light regime.

Lastly we introduce the two-photon correlation $g^{(2)}_{\rm p}(z,t) = \frac{\langle\hat{\mathcal{E}}^\dagger_{\rm p}(z,t)\hat{\mathcal{E}}^\dagger_{\rm p}(z,t)\hat{\mathcal{E}}_{\rm p}(z,t)\hat{\mathcal{E}}_{\rm p}(z,t)\rangle}{\langle\hat{\mathcal{E}}^\dagger_{\rm p}(z,t)\hat{\mathcal{E}}_{\rm p}(z,t)\rangle\langle\hat{\mathcal{E}}^\dagger_{\rm p}(z,t)\hat{\mathcal{E}}_{\rm p}(z,t)\rangle}$ in order to quantify the modification of photon statistics based on the dipole-blockade effect:

$$\begin{aligned}&\partial_z g^{(2)}_{\rm p}(z,t)\\ &= -\Sigma_{RR}(z,t)\,{\rm Im}\left[\frac{P^{(3)}(z,t)-P^{(4)}(z,t)}{\Omega_{\rm p}(z,t)}\right]g^{(2)}_{\rm p}(z,t). \quad (8)\end{aligned}$$

3. Results and discussion

In this section, we show the dual channel storage and retrieval processes by numerical calculations via the dynamic Rydberg-EIT technique. The medium of length $L = 800$ μm consists of cold ^{87}Rb atoms with density $N = 7.5\times10^{11}$ cm^{-3}. The corresponding states are $|g\rangle \equiv |5S_{1/2}, F = 1\rangle$, $|m\rangle \equiv |5S_{1/2}, F = 2\rangle$, $|e\rangle \equiv |5P_{3/2}, F = 2\rangle$, and $|r\rangle \equiv |60S_{1/2}\rangle$, with $\gamma_e = 6.0\times2\pi$ MHz, $\gamma_r = 1.0$ kHz, and $C_6 = 1.4\times10^{11}\times 2\pi$ s^{-1}μm^{-1}. The sequence of the probe and control fields is shown in Fig. 2(a).

The simulation proceed from a Gaussian shape incident probe field with amplitude $\Omega_{\rm p}(0,t) = \Omega^m_{\rm p}\,{\rm e}^{-(t-t_0)^2/\delta t^2}$, detuning $\Delta_{\rm p} = 0$ MHz and two-photon correlation $g^{(2)}_{\rm p}(0,t) = 1.0$, where $t_0 = 1.25$ μs, and $\delta t = 0.5$ μs. At the beginning we apply two control fields with amplitudes $\Omega_{\rm c} = \Omega_{\rm d} = 5.0\times 2\pi$ MHz. Meanwhile, the probe field propagates at a slow group velocity, indicating the formation of the two-mode dark-state polariton (DSP) $\Psi(z,t) = \Psi_{\rm TDP}(z,t) + \Psi_{\rm RDP}(z,t)$ with

$$\begin{aligned}\Psi_{\rm TDP}(z,t) &= {\rm e}^{{\rm i}\Delta_{\rm c}t}\,[1-\Sigma_{RR}(z,t)]\cos\theta(z,t)\Omega_{\rm p}(z,t)\\ &\quad -\sin\theta(z,t)\sqrt{1-\Sigma_{RR}(z,t)}S_1(z,t),\\ \Psi_{\rm RDP}(z,t) &= {\rm e}^{-{\rm i}\Delta_{\rm d}t}\Sigma_{RR}(z,t)\cos\theta(z,t)\Omega_{\rm p}(z,t)\\ &\quad -\sin\theta(z,t)\sqrt{\Sigma_{RR}(z,t)}S_2(z,t), \quad (9)\end{aligned}$$

where $\tan\theta(z,t) = g\sqrt{N/\left(\Omega^2_{\rm c}(t)+\Omega^2_{\rm d}(t)\right)}$. In this propagation process, the corresponding blockade radius is $R_{\rm b} \simeq 4.51$ μm and each SA contains on average $n_{\rm sa} \simeq 384$ atoms. Subsequently, we turn off two control fields adiabatically, then the probe field is completely mapped on the spin fields S_1 and S_2, indicating the dual channel light storage process. In the following, we consider the retrieval process including two cases as shown in Fig. 2(a). In case A, we turn on the control fields simultaneously and retrieve one beam of light, in which the blockade radius $R_{\rm b}$ does not change. In case B, the control fields are applied separately, thus we can get two beams of light. In this procedure, the blockade radius $R_{\rm b} \simeq 5.06$ μm and each SA contains on average $n_{\rm sa} \simeq 543$ atoms. It is noteworthy that the two storage channels are not identical as S_2 is the Rydberg spin field showing the different properties compared with the trivial spin field S_1 arising from the dipole-blockade effect. As a consequence, the two beams of light we get from the sample exit will exhibit different properties, and the storage process is expected to realize the beam splitter.

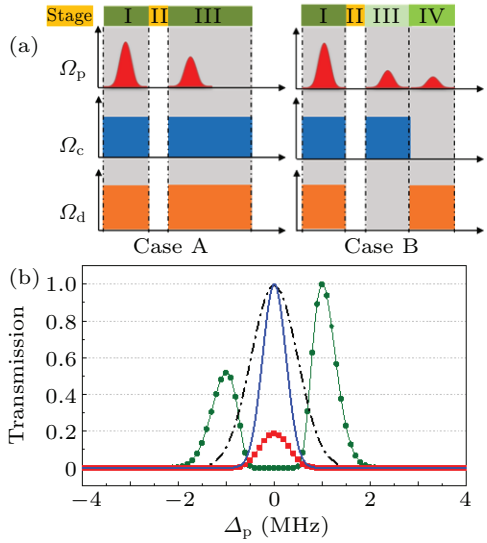


Fig. 2. (a) The sequences of the storage and retrieval processes in different cases. Stages I and Ⅱ in both the cases correspond to the input and storage procedures of pulses, respectively. Stage Ⅲ in case A corresponds simultaneous retrieval, while stages Ⅲ and Ⅳ in case B correspond to separate retrieval processes. (b) Transmission spectrum in different retrieval cases for $\Omega_{\rm c} = \Omega_{\rm d} = 5.0\times2\pi$ MHz with $\Delta_{\rm c} = \Delta_{\rm d} = 0$ MHz (black dash-dotted), $\Omega_{\rm c} = 5.0\times2\pi$, $\Omega_{\rm d} = 0$ MHz with $\Delta_{\rm c} = \Delta_{\rm d} = 0$ MHz (blue solid), $\Omega_{\rm c} = 0$ MHz, $\Omega_{\rm d} = 5.0\times2\pi$ MHz with $\Delta_{\rm c} = \Delta_{\rm d} = 0$ MHz (red square) and $\Omega_{\rm c} = \Omega_{\rm d} = 5.0\times2\pi$ MHz with $\Delta_{\rm c} = \Delta_{\rm d} = 1.0\times2\pi$ MHz (olive circle). Relevant parameters are given at the beginning of Section 3 except $\Omega^m_{\rm p} = 0.1\times2\pi$ MHz.

In Fig. 2(b), we show the transmission spectrum of the system in different retrieval cases. If we apply two control fields with amplitudes $\Omega_{\rm c} = \Omega_{\rm d} = 5.0\times2\pi$ MHz and detunings $\Delta_{\rm c} = \Delta_{\rm d} = 1.0\times2\pi$ MHz, there will exist two EIT windows centered at $\Delta_{\rm p} = \Delta_{\rm c} = 1.0\times2\pi$ MHz and $\Delta_{\rm p} = -\Delta_{\rm d} = -1.0\times2\pi$ MHz, respectively [shown as the olive solid curve with circles in Fig. 2(b)]. However, if we consider the resonance control fields, which means $\Delta_{\rm c} = \Delta_{\rm d} = 0$ MHz, the two EIT windows merge and the degenerate window is centered at $\Delta_{\rm p} = 0$ MHz [black dash-dotted curve in Fig. 2(b)]. In addition, if we apply the single control field $\Omega_{\rm c}$ ($\Omega_{\rm d}$) with

$\Delta_c = 0$ MHz ($\Delta_d = 0$ MHz), the transmission spectrum of the system shows only one EIT window [blue solid curve and red solid curve with squares in Fig. 2(b)]. As the EIT window of the red solid curve is caused by the Rydberg state $|r\rangle$, the peak value of the red solid curve is smaller than the blue one, indicating the dipole-blockade effect. It is also notable that the widths of the EIT windows in different cases are not same, leading to different broadenings of the probe field.

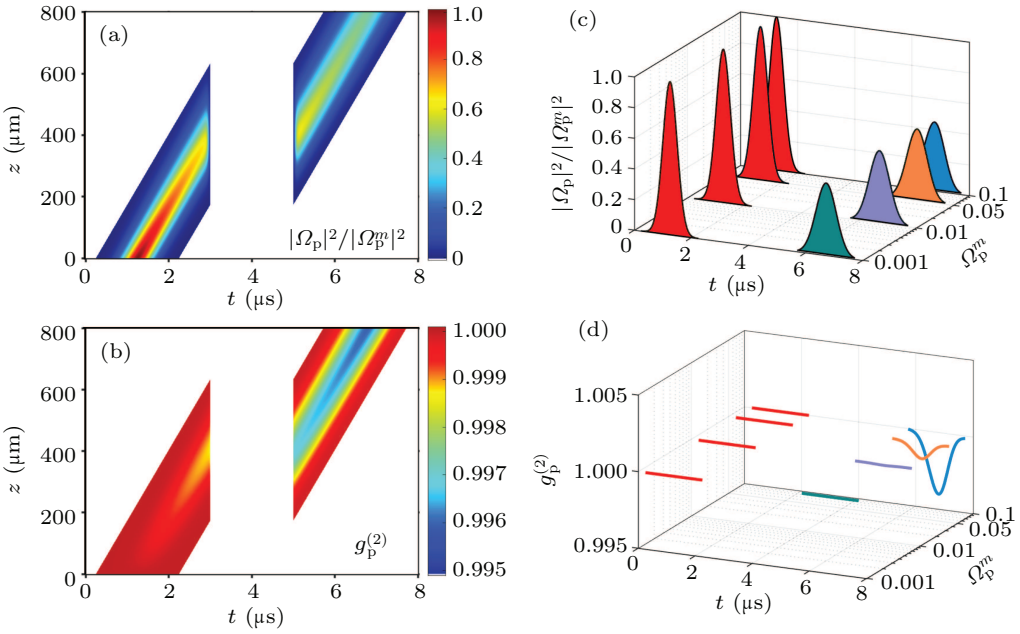


Fig. 3. Dynamic evolution of the scaled light intensity (a) and the two-photon correlation (b) for the incident probe pulse with $\Omega_p^m = 0.1 \times 2\pi$ MHz. Intensity profile (c) and two-photon correlation (d) of the probe field at the sample entrance (left) and exit (right) as functions of time with different input intensities ($\Omega_p^m/2\pi = 0.001$ MHz, 0.01 MHz, 0.05 MHz, 0.1 MHz). The control field sequence is shown in case A (Fig. 2(a)) and relevant parameters are the same as those in Fig. 2 except $\Delta_c = \Delta_d = 0$.

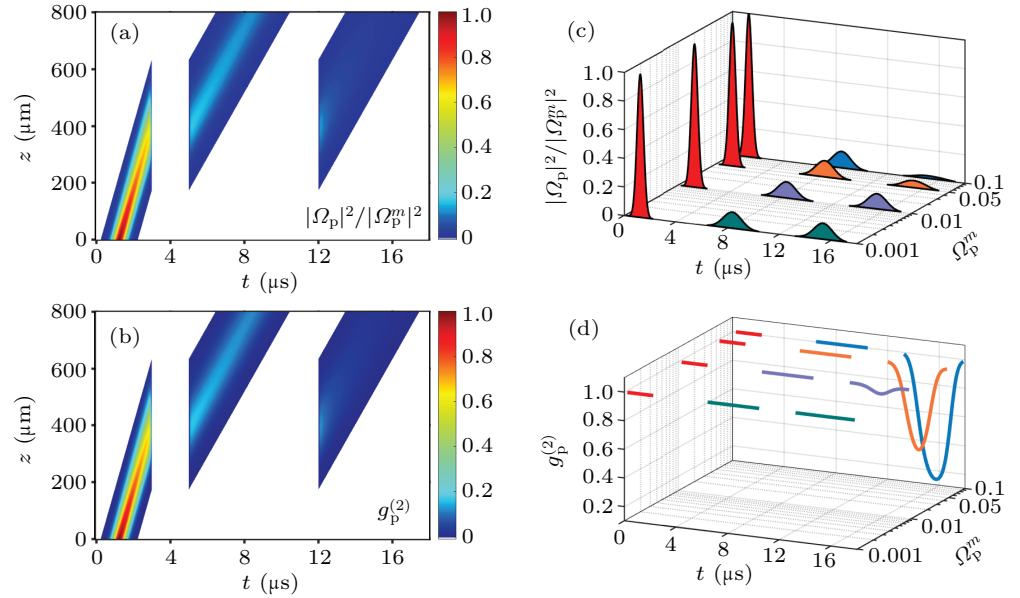


Fig. 4. Dynamic evolution of the scaled light intensity (a) and the two-photon correlation (b) for the incident probe pulse with $\Omega_p^m = 0.1 \times 2\pi$ MHz. Intensity profile (c) and two-photon correlation (d) of the probe field at the sample entrance (left) and exit (right) as functions of time with different input intensities ($\Omega_p^m/2\pi = 0.001$ MHz, 0.01 MHz, 0.05 MHz, 0.1 MHz). The control field sequence is shown in case B and other relevant parameters are the same as those in Fig. 3.

Figure 3 shows the evolution of the probe field intensity and two-photon correlation during the storage and retrieval processes of case A. We can see that the probe field propagates at a slow group velocity of $v_g \approx 230$ m/s when the control fields are switched on (stage I). If we turn off the control fields, the probe light is stored in the medium via two channels: one is the trivial spin field (S_1) channel and the other is the Rydberg spin field (S_2) channel. Hereafter, we turn on the two control fields together with amplitudes $\Omega_c = \Omega_d = 5.0 \times 2\pi$ MHz and detunings $\Delta_c = \Delta_d = 0$ MHz. It can be seen that the stored probe field is released at the sample exit. The steady transmission spectrum of the retrieval process is shown as the black

dash-dotted curve in Fig. 2(b) and we can find only one EIT window centered at $\Delta_p = 0$ MHz. Figures 3(a) and 3(b) show that the loss of the storage is not so serious and the two-photon correlation does not change obviously. In Figs. 3(c) and 3(d), we also check how the light intensity and the two-photon correlation change with the probe intensity to examine the cooperative optical nonlinearity. However, we find that both of them seem to be almost immune to the probe intensity which is well explained in Ref. [45] that when two EIT windows merge in the inverted-Y configuration, the linear optical response overwhelms the cooperative optical nonlinearity. This is very different from the storage process of the ladder configuration.[42]

Figure 4 shows the evolution of the probe field intensity and two-photon correlation during the storage and retrieval processes of case B. The storage process is exactly the same as that in case A while the difference mainly appears in the retrieval process. First, we switch on the control field Ω_c to retrieve the light stored through the trivial spin channel. Then, after the first retrieval process finished, we switch on the control field Ω_d to retrieve the light stored via the Rydberg spin channel. The steady transmission spectrum of the retrieval process is shown by the blue solid curve (trivial spin channel) and the red solid curve (Rydberg spin channel) in Fig. 2(b). It is notable that the transmission window caused by Rydberg state is lower than the trivial window, leading to the unbalanced losses for the two retrieval processes as shown in Fig. 4(a). From Figs. 4(a) and 4(b), it is obvious that the light retrieved from the Rydberg spin channel is weaker than that from the trivial spin channel and the two-photon correlation changes only in the Rydberg retrieval channel. It is also shown that the group velocity of the retrieved light changes to $v_g \approx 115$ m/s in case B. From Figs. 4(c) and 4(d), we notice that the cooperative optical nonlinearity exists in the Rydberg retrieval channel, which is illustrated by the fact that the retrieved light intensity and the two-photon correlation are sensitive to the incident probe intensity. When the probe intensity is weak, the nonlinearity is not so obvious owing to the low excitation probability of the Rydberg state. Moreover, comparing Fig. 4(a) (Fig. 4(c)) with Fig. 3(a) (Fig. 3(c)), we can see that the temporal broadening in case B is much more evident than that in case A. This can be explained by the width of the EIT window. Figure 2(a) shows that the EIT window is narrower if we switch on the control fields separately compared with the simultaneous retrieval case. Thus the sideband frequency losses for the probe field are much larger in the separated retrieval process (case B), resulting in the wider broadening in time domain.

Further we calculate the retrieved field energy versus the input field energy in different retrieval cases in Fig. 5. One of the most obvious features we observe is that only the field energy retrieved from the Rydberg spin channel in case B varies nonlinearly with the increase of the input field energy. However, the field energy retrieved in case A or retrieved from trivial spin channel in case B shows the linear increasing versus input field energy. The reason is intuitionistic. With the stronger input field, the number of the stored photon becomes larger, thus the retrieved field energy increases. The retrieved light propagates in the medium with the transmissivity T. In case A and the trivial retrieval channel of case B, the system shows the linear EIT behavior, indicating that T does not change obviously with probe intensity varying, so the energy we get from the sample exit varies linearly with the increasing input field energy. The nonlinear behavior is caused directly by the Rydberg blockade effect. Specifically, the transmissivity T of the Rydberg retrieval channel in case B exhibits cooperative nonlinearity with the incident probe intensity owing to the blockade effect,[45] which manifests that T decreases with the increasing probe intensity. Then the retrieved light from the Rydberg spin channel in case B will experience nonlinear absorption with the increasing input field energy.[34]

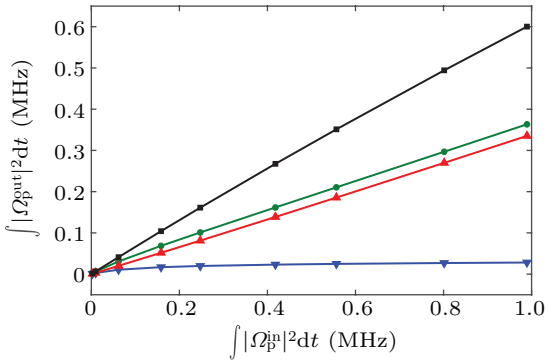


Fig. 5. Retrieved field energy versus input field energy for case A (black square), case B (olive circle), trivial storage channel in case B (red upper triangular) and Rydberg storage channel in case B (blue lower triangular). Other parameters are the same as those in Figs. 3 and 4, except that $\Omega_p^m/2\pi$ is increased from zero up to 0.2 MHz.

Comparing the black solid curve with the olive solid curve, we can see that the total retrieved field energy in case A is larger than that in case B, which can be well explained by the following considerations. For one thing, from Fig. 2(b) we notice that if we apply two resonant control fields together, the EIT window is wider than the case of applying just one control field, so the losses of the sideband frequencies are larger for the separate retrieval process (case B). For the other, we have shown in Fig. 2(b) that the EIT window caused by the the Rydberg state $|r\rangle$ for the separate retrieval process (case B) is lower than the EIT window for the simultaneous retrieval process (case A), resulting in the serious loss for the separate retrieval process (case B). Moreover, comparing Fig. 3(a) with Fig. 4(a), we can see that the group velocity of the retrieval light for the separate retrieval process (case B) is slower than that for the simultaneous retrieval process (case A), which means that the light stays in the medium longer for the separate retrieval process (case B), leading to more loss.

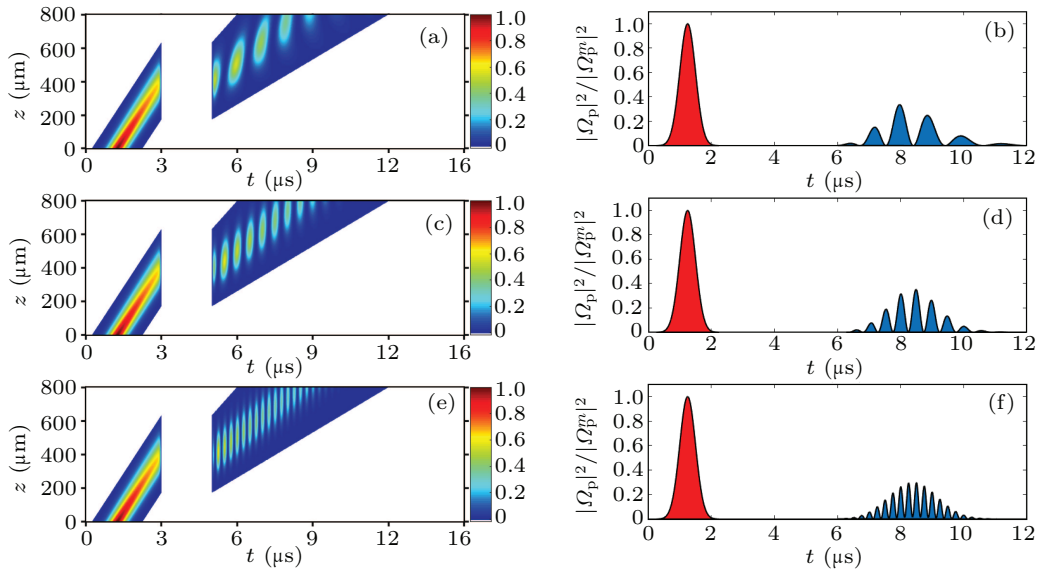


Fig. 6. Dynamic evolution of the probe field intensity inside the cold atomic sample [(a), (c), (e)] and the probe field intensity at the sample entrance and exit as a function of time t [(b), (d), (f)] for the incident probe pulse with $\Omega_p^m = 0.1 \times 2\pi$ MHz. The two control fields with $\Omega_c = \Omega_d = 5 \times 2\pi$ MHz and $\Delta_c = \Delta_d = 0$ MHz are applied for the first 3 μs. Then we turn off the control fields and after 2 μs storage, we turn on the control fields with amplitudes $\Omega_c = \Omega_d = 5 \times 2\pi$ MHz and detunings $\Delta_c = \Delta_d = 0.5 \times 2\pi$ MHz [(a), (b)], $\Delta_c = \Delta_d = 1.0 \times 2\pi$ MHz [(c), (d)], and $\Delta_c = \Delta_d = 2.0 \times 2\pi$ MHz [(e), (f)]. Other parameters are the same as those in Fig. 3.

Overall, by adjusting the different control field sequences, we can retrieve the beams of light with different properties. On the one hand, if we switch on the control fields simultaneously (case A), we can get only one beam of light with little loss and the retrieved field energy shows linear dependence against the input field energy. On the other hand, if we switch on the control fields separately (case B), we can get two beams of light with different properties. Firstly, the retrieved light from trivial spin channel experiences little loss while the retrieved light from Rydberg spin channel is greatly attenuated in intensity accompanied by the anti-bunching feature. Secondly, the intensity and the two-photon correlation are immune (sensitive) to the incident probe intensity for the light retrieved from trivial spin (Rydberg spin). With the increase of the incident intensity, the loss and the anti-bunching effect become stronger for the light retrieved from Rydberg spin. Thirdly, the retrieved field energy from the trivial spin channel is linearly dependent while that from the Rydberg spin channel is nonlinearly dependent on the input field energy. Also, the energy retrieved from the Rydberg spin will show an intriguing saturation effect.

In the following, we show the generation and manipulating of the beating signal in the dual channel storage and retrieval processes. In order to generate the beating signal, we need to make the system work in case A. Notably, we apply two resonant control fields at the beginning, but the control fields applied in the retrieval process are detuned. In Fig. 6, we show how the light intensity evolves in this process and we also compare the cases with different retrieval control field detunings. We choose $\Delta_c = \Delta_d = 0.5 \times 2\pi$ MHz in (a) and (b), $\Delta_c = \Delta_d = 1 \times 2\pi$ MHz in (c) and (d), and $\Delta_c = \Delta_d = 2 \times 2\pi$ MHz in (e) and (f). It is clear that we can get the beating signal at the sample exit. We also note that the retrieved field intensity oscillates fast with the increase of $|\Delta_c + \Delta_d|$.[8] Thus, by adjusting the detunings of the control fields, we can manipulate the beating frequency. DSP $\Psi(z,t)$, which is defined at the beginning of Section 3, helps to gain a deeper insight into the physical description for the generation of beating signal. Equation (9) shows that the slow TDP and RDP will turn into the fast probe fields $e^{i\Delta_c t}[1-\Sigma_{RR}(z,t)]\Omega_p(z,t)$ and $e^{-i\Delta_d t}\Sigma_{RR}(z,t)\Omega_p(z,t)$, respectively. If the detunings of the retrieval fields are nonzero, the fields converted from TDP and RDP gain phases and interfere with each other, indicating the generation of perfect beating signal which is the manifestation of the first order correlation. Here we give the detailed calculation for the beating frequency ω_B. In the retrieval process, if the detuned coupling fields are applied simultaneously, the fast probe field parts $e^{i\Delta_c t}[1-\Sigma_{RR}(z,t)]\Omega_p(z,t)$ and $e^{-i\Delta_d t}\Sigma_{RR}(z,t)\Omega_p(z,t)$ in the slow TDP and RDP will convert into the field, and then we can get the superposed field

$$\begin{aligned} & e^{i\Delta_c t}[1-\Sigma_{RR}(z,t)]\Omega_p(z,t)\, e^{i(k_p z-\omega_p t)} \\ & + e^{-i\Delta_d t}\Sigma_{RR}(z,t)\Omega_p(z,t)\, e^{i(k_p z-\omega_p t)} + \text{c.c.} \\ & = A(z,t)\, e^{i\left(\frac{\Delta_c-\Delta_d}{2}t+\phi\right)}\Omega_p(z,t)\, e^{i(k_p z-\omega_p t)} + \text{c.c.}, \end{aligned} \tag{10}$$

with

$$A(z,t) = \sqrt{1+2\Sigma_{RR}^2(z,t)\,(1-\Sigma_{RR}(z,t))\,(1+\cos[(\Delta_c+\Delta_d)t])}$$

and $\tan\phi = [1-2\Sigma_{RR}(z,t)]\tan(\frac{\Delta_c+\Delta_d}{2}t)$, calculated according to the field superposition principle. Choosing $\Delta_c = \Delta_d$, we can

get the retrieval field $A(z,t)\Omega_{\rm p}(z,t)\,{\rm e}^{{\rm i}\left(k_{\rm p}z-\omega_{\rm p}t+\phi\right)}+{\rm c.c.}$ Obviously, the intensity of the retrieved field $|A(z,t)\Omega_{\rm p}|^2$ will oscillate with the frequency $\omega_{\rm B}=|\Delta_{\rm c}+\Delta_{\rm d}|$, which can be certified in Fig. 6.

4. Conclusions

In summary, we have studied the dual channel storage and retrieval processes in Rydberg atomic ensemble with inverted-Y configuration by adopting the SA theory. It is found that the retrieval for single or double beams of light pulse is achievable by modulating the control fields. Turning on the control fields simultaneously means the retrieval for one beam of light pulse which experiences little loss. One can retrieve two beams of light pulse with different intensities and different statistical properties by switching on the control fields separately. The light read out from the Rydberg spin channel is greatly attenuated in intensity and shows cooperative optical nonlinearity as a consequence of dipole-blockade effect in Rydberg-EIT medium. The dipole-blockade effect also leads to the nonlinear dependence on the input field energy for the retrieved field energy from the Rydberg spin channel. Moreover, it is viable to generate beating signal in this system by applying nonresonant control fields and the beating frequency is determined by the detunings of the control fields. Thus the system can be used to realize the light manipulation. The application is not only limited to store light information. It is also expected to split the light into two beams with different properties, to generate and control the beating signal. We also expect to achieve the other precise light manipulation in Rydberg atomic ensemble.

Appendix A: Rydberg excitation of superatom

It is obvious that $|G\rangle$ and first-order collective states ($|E^{(1)}\rangle$, $|M^{(1)}\rangle$ and $|R^{(1)}\rangle$) could form a four-level inverted-Y configuration of superatom, neglecting other higher-order collective states safely in the weak probe limit. At this time, the Rydberg excitation probability in an SA is similar to that of a single atom. For a single atom with inverted-Y configuration, we have the Heisenberg Langevin equations:

$$\begin{aligned}
&\partial_t\hat{\rho}_{gg}(z,t)=2\gamma_e\hat{\rho}_{ee}(z,t)-{\rm i}\hat{\Omega}_{\rm p}(z,t)\hat{\rho}_{eg}(z,t)+{\rm i}\hat{\Omega}_{\rm p}^{\dagger}(z,t)\hat{\rho}_{ge}(z,t),\\
&\partial_t\hat{\rho}_{mm}(z,t)=2\gamma_e\hat{\rho}_{ee}(z,t)-{\rm i}[\Omega_{\rm c}(t)\hat{\rho}_{em}(z,t)-\Omega_{\rm c}^{*}(t)\hat{\rho}_{em}(z,t)],\\
&\partial_t\hat{\rho}_{rr}(z,t)=-2\gamma_r\hat{\rho}_{rr}(z,t)+{\rm i}[\Omega_{\rm d}(t)\hat{\rho}_{re}(z,t)-\Omega_{\rm d}^{*}(t)\hat{\rho}_{er}(z,t)],\\
&\partial_t\hat{\rho}_{gm}(z,t)={\rm i}(\Delta_{\rm p}-\Delta_{\rm c})\hat{\rho}_{gm}(z,t)-{\rm i}\hat{\Omega}_{\rm p}(z,t)\hat{\rho}_{em}(z,t)+{\rm i}\Omega_{\rm c}^{*}(t)\hat{\rho}_{ge}(z,t),\\
&\partial_t\hat{\rho}_{ge}(z,t)=-[\gamma_e-{\rm i}\Delta_{\rm p}]\hat{\rho}_{ge}(z,t)+{\rm i}\hat{\Omega}_{\rm p}(z,t)\left[\hat{\rho}_{gg}(z,t)-\hat{\rho}_{ee}(z,t)\right]+{\rm i}\Omega_{\rm c}(t)\hat{\rho}_{gm}(z,t)+{\rm i}\Omega_{\rm d}^{*}(t)\hat{\rho}_{gr}(z,t),\\
&\partial_t\hat{\rho}_{gr}(z,t)=-\left[\gamma_r-{\rm i}\left(\Delta_{\rm p}+\Delta_{\rm d}\right)\right]\hat{\rho}_{gr}(z,t)-{\rm i}\hat{\Omega}_{\rm p}(z,t)\hat{\rho}_{er}(z,t)+{\rm i}\Omega_{\rm d}(t)\hat{\rho}_{ge}(z,t),\\
&\partial_t\hat{\rho}_{me}(z,t)=-[\gamma_e-{\rm i}\Delta_{\rm c}]\hat{\rho}_{me}(z,t)+{\rm i}\hat{\Omega}_{\rm p}(z,t)\hat{\rho}_{mg}(z,t)+{\rm i}\Omega_{\rm d}^{*}(t)\hat{\rho}_{mr}(z,t)+{\rm i}\Omega_{\rm c}(t)\left[\hat{\rho}_{mm}(z,t)-\hat{\rho}_{ee}(z,t)\right],\\
&\partial_t\hat{\rho}_{mr}(z,t)=-\left[\gamma_r-{\rm i}\left(\Delta_{\rm c}+\Delta_{\rm d}\right)\right]\hat{\rho}_{mr}(z,t)-{\rm i}\Omega_{\rm c}(t)\hat{\rho}_{er}(z,t)+{\rm i}\Omega_{\rm d}(t)\hat{\rho}_{me}(z,t),\\
&\partial_t\hat{\rho}_{er}(z,t)=-[\gamma_e+\gamma_r-{\rm i}\Delta_{\rm d}]\hat{\rho}_{er}(z,t)-{\rm i}\hat{\Omega}_{\rm p}^{\dagger}(z,t)\hat{\rho}_{gr}(z,t)-{\rm i}\Omega_{\rm c}^{*}(t)\hat{\rho}_{mr}(z,t)+{\rm i}\Omega_{\rm d}(t)\left[\hat{\rho}_{ee}(z,t)-\hat{\rho}_{rr}(z,t)\right].
\end{aligned}\tag{A1}$$

Also, note that, in an SA, the probe (coupling) coefficients are $\sqrt{n_{\rm sa}}\hat{\Omega}_{\rm p}$ ($\Omega_{\rm c}$, $\Omega_{\rm d}$) on transition $|G\rangle\rightarrow|E^{(1)}\rangle$ ($|E^{(1)}\rangle\rightarrow|M^{(1)}\rangle$, $|E^{(1)}\rangle\rightarrow|R^{(1)}\rangle$); $\sqrt{2(n_{\rm sa}-1)}\hat{\Omega}_{\rm p}$ ($\sqrt{2}\Omega_{\rm c}$, $\sqrt{2}\Omega_{\rm d}$) on transition $|E^{(1)}\rangle\rightarrow|E^{(2)}\rangle$ ($|E^{(2)}\rangle\rightarrow|E^{(1)}M^{(1)}\rangle$, $|E^{(2)}\rangle\rightarrow|E^{(1)}R^{(1)}\rangle$); $\sqrt{n_{\rm sa}-1}\hat{\Omega}_{\rm p}$ ($\sqrt{2}\Omega_{\rm c}$, $\Omega_{\rm d}$) on transition $|M^{(1)}\rangle\rightarrow|E^{(1)}M^{(1)}\rangle$ ($|E^{(1)}M^{(1)}\rangle\rightarrow|M^{(2)}\rangle$, $|E^{(1)}M^{(1)}\rangle\rightarrow|M^{(1)}R^{(1)}\rangle$), etc. In this case, we obtain $\langle\hat{\Sigma}_{RR}(z)\rangle=\langle\hat{\Sigma}_{RR}^{(1)}(z)\rangle+\langle\hat{\Sigma}_{RR}^{(2)}(z)\rangle+\langle\hat{\Sigma}_{RR}^{(3)}(z)\rangle+\cdots$, with the first-, second-, and third-order components. As we notice from Eq. (A1), dynamic evolutions of these operators are accompanied with the replacement of $\hat{\Omega}_{\rm p}^{\dagger}(z)\hat{\Omega}_{\rm p}(z)\rightarrow\eta_{\rm p}\hat{\Omega}_{\rm p}^{\dagger}(z)\hat{\Omega}_{\rm p}(z)$, $|\Omega_{\rm c}|^2\rightarrow\eta_{\rm c}|\Omega_{\rm c}|^2$ and $|\Omega_{\rm d}|^2\rightarrow\eta_{\rm d}|\Omega_{\rm d}|^2$ with $\eta_{\rm p}$, $\eta_{\rm c}$, $\eta_{\rm d}$ being the corresponding substitution coefficients. Thus, compared to the single atomic counterpart $\langle\hat{\rho}_{\kappa\kappa}(z)\rangle=\overline{\rho}_{\kappa\kappa}[\hat{\Omega}_{\rm p}^{\dagger}(z)\hat{\Omega}_{\rm p}(z),|\Omega_{\rm c}|^2,|\Omega_{\rm d}|^2]$, with $\kappa\in\{e,r,m\}$, each order steady-state populations of SA can be expressed as

$$\begin{aligned}
&\langle\hat{\Sigma}_{EE}^{(1)}(z)\rangle=\overline{\rho}_{ee}[n_{\rm sa}\hat{\Omega}_{\rm p}^{\dagger}(z)\hat{\Omega}_{\rm p}(z),|\Omega_{\rm c}|^2,|\Omega_{\rm d}|^2],\\
&\langle\hat{\Sigma}_{MM}^{(1)}(z)\rangle=\overline{\rho}_{mm}[n_{\rm sa}\hat{\Omega}_{\rm p}^{\dagger}(z)\hat{\Omega}_{\rm p}(z),|\Omega_{\rm c}|^2,|\Omega_{\rm d}|^2],\quad\langle\hat{\Sigma}_{RR}^{(1)}(z)\rangle=\overline{\rho}_{rr}[n_{\rm sa}\hat{\Omega}_{\rm p}^{\dagger}(z)\hat{\Omega}_{\rm p}(z),|\Omega_{\rm c}|^2,|\Omega_{\rm d}|^2],\\
&\langle\hat{\Sigma}_{RR}^{(2)}(z)\rangle=\langle\hat{\Sigma}_{MM}^{(1)}(z)\rangle\cdot\overline{\rho}_{rr}[(n_{\rm sa}-1)\hat{\Omega}_{\rm p}^{\dagger}\hat{\Omega}_{\rm p},2|\Omega_{\rm c}|^2,|\Omega_{\rm d}|^2]+\langle\hat{\Sigma}_{EE}^{(1)}(z)\rangle\cdot\overline{\rho}_{rr}[2(n_{\rm sa}-1)\hat{\Omega}_{\rm p}^{\dagger}\hat{\Omega}_{\rm p},2|\Omega_{\rm c}|^2,2|\Omega_{\rm d}|^2],\\
&\langle\hat{\Sigma}_{RR}^{(3)}(z)\rangle=\langle\hat{\Sigma}_{MM}^{(1)}(z)\rangle\cdot\overline{\rho}_{mm}[(n_{\rm sa}-1)\hat{\Omega}_{\rm p}^{\dagger}\hat{\Omega}_{\rm p},2|\Omega_{\rm c}|^2,|\Omega_{\rm d}|^2]\cdot\overline{\rho}_{rr}[(n_{\rm sa}-2)\hat{\Omega}_{\rm p}^{\dagger}\hat{\Omega}_{\rm p},3|\Omega_{\rm c}|^2,|\Omega_{\rm d}|^2]\\
&\qquad+\langle\hat{\Sigma}_{MM}^{(1)}(z)\rangle\cdot\overline{\rho}_{ee}[(n_{\rm sa}-1)\hat{\Omega}_{\rm p}^{\dagger}\hat{\Omega}_{\rm p},2|\Omega_{\rm c}|^2,|\Omega_{\rm d}|^2]\cdot\overline{\rho}_{rr}[2(n_{\rm sa}-2)\hat{\Omega}_{\rm p}^{\dagger}\hat{\Omega}_{\rm p},4|\Omega_{\rm c}|^2,2|\Omega_{\rm d}|^2]\\
&\qquad+\langle\hat{\Sigma}_{EE}^{(1)}(z)\rangle\cdot\overline{\rho}_{ee}[2(n_{\rm sa}-1)\hat{\Omega}_{\rm p}^{\dagger}\hat{\Omega}_{\rm p},2|\Omega_{\rm c}|^2,2|\Omega_{\rm d}|^2]\cdot\overline{\rho}_{rr}[3(n_{\rm sa}-2)\hat{\Omega}_{\rm p}^{\dagger}\hat{\Omega}_{\rm p},3|\Omega_{\rm c}|^2,3|\Omega_{\rm d}|^2].
\end{aligned}\tag{A2}$$

Acknowledgements

Project supported by the National Natural Science Foundation of China (Grant No. 12104107), the Natural Science Foundation of Guangxi Province, China (Grant No. AD19245180), the Natural Science Foundation of Jilin Province, China (Grant No. 20220101009JC), and the "Yucai Project" of Guangxi Normal University.

References

[1] Lukin M D 2003 *Rev. Mod. Phys.* **75** 457
[2] Fleischhauer M, Imamoglu A and Marangos J P 2005 *Rev. Mod. Phys.* **77** 633
[3] Fleischhauer M and Lukin M D 2000 *Phys. Rev. Lett.* **84** 5094
[4] Ma L J, Slattery O and Tang X 2017 *J. Opt.* **19** 043001
[5] Schraft D, Hain M, Lorenz N and Halfmann T 2016 *Phys. Rev. Lett.* **116** 073602
[6] Iakoupov I, Borregaard J and Sørensen A S 2018 *Phys. Rev. Lett.* **120** 010502
[7] Wang H, Li S J, Xu Z X, Zhao X B, Zhang L J, Li J H, Wu Y L, Xie C D, Peng K C and Xiao M 2011 *Phys. Rev. A* **83** 043815.
[8] Bao Q Q, Gao J W, Cui C L, Wang G, Xue Y and Wu J H 2011 *Opt. Express* **12** 11832
[9] Bajcsy M, Zibrov A S and Lukin M D 2003 *Nature* **426** 638
[10] Bao Q Q, Zhang X H, Gao J Y, Zhang Y, Cui C L and Wu J H 2011 *Phys. Rev. A* **84** 063812
[11] Saffman M, Walker T G and Mølmer K 2010 *Rev. Mod. Phys.* **82** 2313
[12] Wu X L, Liang X H, Tian Y Q, Yang F, Chen C, Liu Y C, Tey M K and You L 2021 *Chin. Phys. B* **30** 020305
[13] Zhang Z Y, Ding D S and Shi B S 2021 *Chin. Phys. B* **30** 020307
[14] Gorshkov A V, Otterbach J, Fleischhauer M, Pohl T and Lukin M D 2011 *Phys. Rev. Lett.* **107** 133602
[15] Petrosyan D, Otterbach J and Fleischhauer M 2011 *Phys. Rev. Lett.* **107** 213601
[16] Tebben A, Hainaut C, Walther V, Zhang Y C, Zürn G, Pohl T and Weidemüller M 2019 *Phys. Rev. A* **100** 063812
[17] Müller M M, Murphy M, Montangero S, Calarco T, Grangier P and Browaeys A 2014 *Phys. Rev. A* **89** 032334
[18] Wu H Z, Huang X R, Hu C S, Yang Z B and Zheng S B 2017 *Phys. Rev. A* **96** 022321
[19] Li M, Guo F Q, Jin Z, Yan L L, Liang E J and Su S L 2021 *Phys. Rev. A* **103** 062607
[20] Xing T H, Zhao P Z and Tong D M 2021 *Phys. Rev. A* **104** 012618
[21] Rao D D B and Mølmer K 2013 *Phys. Rev. Lett.* **111** 033606
[22] Tian X D, Liu Y M, Cui C L and Wu J H 2015 *Phys. Rev. A* **92** 063411
[23] Hu C S, Lin X Y, Shen L T, Su W J, Jiang Y K, Wu Hu Z and Zheng S B 2020 *Opt. Express* **28** 1492
[24] Li R, Yu D M, Su S L and Qian J 2020 *Phys. Rev. A* **101** 042328
[25] Yang C, Li D X and Shao X Q 2021 *Chin. Phys. B* **30** 023201
[26] Firstenberg O, Peyronel T, Liang Q Y, Gorshkov A V, Lukin M D and Vuletić V 2013 *Nature* **502** 71
[27] Maghrebi M F, Gullans M J, Bienias P, Choi S, Martin I, Firstenberg O, Lukin M D, Büchler H P and Gorshkov A V 2015 *Phys. Rev. Lett.* **115** 123601
[28] Khazali M, Heshami K and Simon C 2017 *J. Phys. B: At. Mol. Opt. Phys.* **50** 215301
[29] Baur S, Tiarks D, Rempe G and Dürr S 2014 *Phys. Rev. Lett.* **112** 073901
[30] Li W and Lesanovsky I 2015 *Phys. Rev. A* **92** 043828
[31] Stiesdal N, Busche H, Kleinbeck K, Kumlin J, Hansen M G, Büchler H P and Hofferberth S 2021*Nat. Commun.* **12** 4328
[32] Maxwell D, Szwer D J, Paredes-Barato D, Busche H, Pritchard J D, Gauguet A, Weatherill K J, Jones M P A and Adams C S 2013 *Phys. Rev. Lett.* **110** 103001
[33] Ripka F, Chen Y H, Löw R and Pfau T 2016 *Phys. Rev. A* **93** 053429
[34] Distante E, Padrón-Brito A, Cristiani M, Paredes-Barato D and de Riedmatten H 2016 *Phys. Rev. Lett.* **117** 113001
[35] Li L and Kuzmich A 2016 *Nat. Commun.* **7** 13618
[36] Distante E, Farrera P, Padrón-Brito A, Paredes-Barato D, Heinze Ge and de Riedmatten H 2017 *Nat. Commun.* **8** 14072
[37] Mirgorodskiy I, Christaller F, Braun C, Paris-Mandoki A, Tresp C and Hofferberth S 2017 *Phys. Rev. A* **96** 011402
[38] Padrón-Brito A, Tricarico R, Farrera P, Distante E, Theophilo K, Chang D and de Riedmatten H 2021 *New J. Phys.* **23** 063009
[39] Gullans M J, Thompson J D, Wang Y, Liang Q Y, Vuletić V, Lukin M D and Gorshkov A V 2016 *Phys. Rev. Lett.* **117** 113601
[40] Yang L, He B, Wu J H, Zhang Z Y and Xiao M 2016 *Optica* **3** 1095
[41] Zeuthen E, Gullans M J, Maghrebi M F and Gorshkov A V 2017 *Phys. Rev. Lett.* **119** 043602
[42] Tian X D, Liu Y M, Bao Q Q, Wu J H, Artoni M and La Rocca G C 2018 *Phys. Rev. A* **97** 043811
[43] Yang F, Liu Y C and You L 2019 *Phys. Rev. A* **99** 063803
[44] Zhang H X, Wu J H, Artoni M and La Rocca G C 2022 *Front. Phys.* **17** 22502
[45] Yan D, Liu Y M, Bao Q Q, Fu C B and Wu J H 2012 *Phys. Rev. A* **86** 023828
[46] Yan D, Cui C L, Liu Y M, Song L J and Wu J H 2013 *Phys. Rev. A* **87** 023827
[47] Gorshkov A V, André A, Lukin M D and Sørensen A S 2007 *Phys. Rev. A* **76** 033805